

# Atomic Cascade in Muonic and Hadronic Hydrogen Atoms

T.S. Jensen, V.P. Popov and V.N. Pomerantsev

*Institute of Nuclear Physics, Moscow State University, 119992 Moscow, Russia<sup>a</sup> Institution1*

## Abstract

The atomic cascade in  $\mu^-p$  and  $\pi^-p$  atoms has been studied with the improved version of the extended cascade model in which new quantum mechanical calculations of the differential and integral cross sections of the elastic scattering, Stark transitions and Coulomb de-excitation have been included for the principal quantum number values  $n \leq 8$  and the relative energies  $E \geq 0.01$  eV. The  $X$ -ray yields and kinetic energy distributions are compared with the experimental data.

## 1 Introduction

The exotic hydrogen-like atoms are formed in highly excited states, when a heavy negative particle ( $\mu^-$ ,  $\pi^-$ ,  $K^-$ , *etc.*) slows down and captures in hydrogen media due to inelastic collisions. The formation is followed by the atomic cascade in which the initial distributions in the quantum numbers ( $n, l$ ) and kinetic energy of the exotic atom change due to various processes: radiative transitions, external Auger effect, elastic scattering, Stark transitions, Coulomb de-excitation, weak decay and nuclear absorption (in case of hadronic atoms). A good understanding of the kinetics of atomic cascade in hydrogen-like exotic atoms is very important both for the planning and interpretation of the experiments (see for a review [1]). The first theoretical study of the atomic cascade was performed more than forty five years ago by Leon and Bethe [2]. In this paper, and later in more refined models [3, 4], the rates of the collisional processes were calculated in the semiclassical approximation at a fixed kinetic energy ( $\sim 1$  eV) and used for the simulation of the atomic cascade. A number of experiments in which the energy distributions of  $\mu^-p$ ,  $\mu^-d$  and  $\pi^-p$  atoms were measured using various time-of-flight methods [5, 6, 7, 8, 9] showed that the kinetic energy changes during the cascade. In particular, the existence of high energy components has been established in pionic hydrogen in the neutron time-of-flight experiment [7] and in muonic hydrogen in diffusion experiments [8, 9]. This experiments require a more sophisticated approach taking the evolution of the kinetic energy distribution into account during the whole atomic cascade. Beginning with Markushin [10] recent cascade models take into account the acceleration and deceleration processes. The extended standard cascade model (ESCM) [11] introduces a number of improvements compared to the earlier models: for example, the scattering from molecular hydrogen at high  $n$  is calculated as opposed to the phenomenological treatment in other cascade models.

In the recent papers [12, 13], the dynamics of the collisions of the excited exotic atoms with hydrogen ones has been studied in the framework of the close-coupling approach. The elastic scattering, Stark transitions and Coulomb de-excitation were described by a unified manner in this approach. The differential and integral cross-sections were calculated in a

wide range of the principle quantum number values and relative energies for muonic, pionic and antiprotonic hydrogen atoms. The vacuum polarization and strong interaction shifts (for hadronic atoms) were taken into account (see also this issue).

In the present paper the first theoretical results of the X-ray yields and kinetic energy distributions for  $\mu^-p$  and  $\pi^-p$  atoms calculated in the new version of the ESCM are introduced. The new results for the collisional processes ([12, 13], see also this issue), especially for Coulomb de-excitation process, are used in the present ESCM and lead to an essential improvement over the previous cascade calculations.

## 2 The extended standard cascade model

The cascade in exotic atoms (as in the previous ESCM) is divided into the classical domain for high  $n$  and the quantum mechanical domain for low  $n$ . In the classical domain (for muonic and pionic hydrogen we use  $n \geq 9$ ) the classical-trajectory Monte Carlo calculations have been included in the cascade model (see for details [11]) with the molecular structure of the target taken into account for the description of the elastic scattering, Stark mixing and Coulomb de-excitation processes. The external Auger effect was calculated in the semiclassical approximation through the whole cascade. In the upper stage of the cascade the distributions in quantum numbers and kinetic energy are calculated. Further, these distributions were used as input data for the next stage of the atomic cascade. In the quantum mechanical domain (at  $n \leq 8$ ) the differential and integral cross sections for all  $nl \mapsto n'l'$  transitions (besides the Auger and radiative de-excitations) were calculated in the fully quantum mechanical close-coupling approach (see [12, 13] and references therein) for the initial states with  $n \leq 8$  and relative energies  $E \geq 0.01$  eV. The corresponding arrays of the cross sections are included in the cascade code. Thus the present cascade code does not employ any fitting parameters and the kinetics of the atomic cascade is treated more accurately.

The initial conditions for the cascade calculations are defined by the initial distributions in the quantum numbers  $n$  and  $l$  and the laboratory kinetic energy of the exotic atoms. In the simplest picture, the exotic particle is captured by the proton of the hydrogen atom in a state with  $n_i \sim \sqrt{M}$  ( $M$  is a reduced mass of exotic atom in atomic units). More elaborate approaches [14, 15] take the molecular effects of the target into account and predict distribution in the initial  $n_i$  with the peak shifted towards lower values and non-statistical  $l_i$ -distribution. In the present cascade calculations the influence of the initial parameters are also studied. In order to obtain good statistics the cascade calculations were performed with  $10^6$  events.

## 3 Results

### 3.1 Muonic hydrogen

Muonic hydrogen atom is the simplest of exotic atoms and its experimental and theoretical studies are the best probe for the investigation of the various processes in exotic atom from hydrogen atom or molecule collisions. The present cascade calculations in muonic hydrogen have been done in the density range  $(10^{-7} - 1)$  (in units of Liquid Hydrogen Density,

$LHD = 4.25 \cdot 10^{22} \text{ atoms/cm}^3$ ) using various initial conditions. The results are compared with the experimental data [16, 17, 18] for relative  $K$  X-ray yields. The energy distributions of muonic hydrogen and Doppler broadening of the X-ray lines are also introduced.

The dependence of the calculated absolute  $K$  X-ray yields on hydrogen density for the  $\mu^-p$  atom are shown in Figure 1.

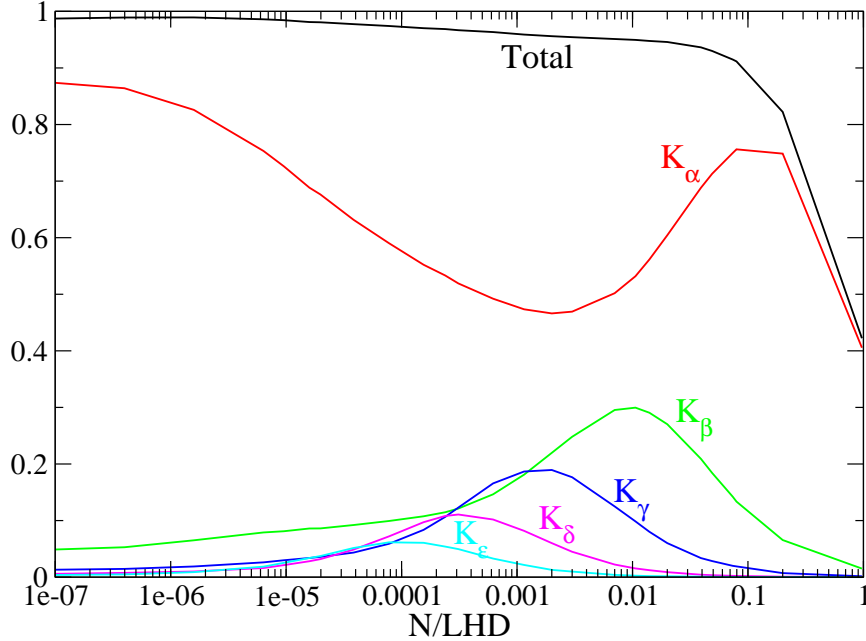


Figure 1: The density dependence of the absolute  $K$  X-ray yields in muonic hydrogen.

In contrast to the practically linear dependence of the absolute  $K_{tot}$  yield on the density in the wide range from  $10^{-7}$  LHD to  $\sim 10^{-2}$  LHD the individual  $K_i$  yields ( $i = \alpha, \beta$ , etc.) have a more complicated density dependence due to the competition between the various collisional and non-collisional processes during the cascade. The atomic cascade at low target densities is mainly dominated by the radiative de-excitation proceeding through the circular states that result in  $2p \rightarrow 1s$  transition whereas the transitions  $np \rightarrow 1s$  are much weaker. We see the corresponding picture in Figure 1. At very low density the kinetic energy distribution of the muonic atom must conserve its initial kinetic energy distribution. While the density is increased the role of the collisional processes enhances leading to both the decrease of  $K_\alpha$  yield and simultaneously the increase of the other  $K_i$  yields ( $i \neq \alpha$ ), conserving the total absolute yield practically unchangeable. With increasing density the Coulomb de-excitation becomes also more efficient (especially at low energies) and leads to the acceleration of the exotic atom and higher populations of the  $np$  states with  $n > 2$  due to the Stark transitions. At the target densities more than  $\sim 10^{-3} \div 10^{-2}$  LHD the collisional de-excitation  $n \rightarrow n' (n' < n)$  begins to dominate the radiative transitions (external Auger effect and Coulomb transitions) resulting in the decrease of the  $K_{\geq \beta}$  yields. Since the collisional de-excitations to the  $1s$  state of the muonic hydrogen are strongly suppressed (more or about 2 keV energy is released) we observe the enhancement of the absolute  $K_\alpha$  yield due to the collisional transitions to  $2p$  state and the Stark  $2s \rightarrow 2p$  transition at the energy above the threshold. Thus the swift suppression of the absolute  $K_\alpha$

yield at the densities from  $10^{-7}$  LHD to  $\sim 10^{-3}$  LHD and increase at more higher densities can be explained by the competition of the different processes during the atomic cascade in which the evolution of the kinetic energy is taken into account through the whole cascade.

The discussed above regularities in the absolute yields can be justified or vice versa in comparison of the calculated relative X-ray yields for the  $\mu^-p$  with the experimental data [16, 17, 18] introduced in Figure 2.

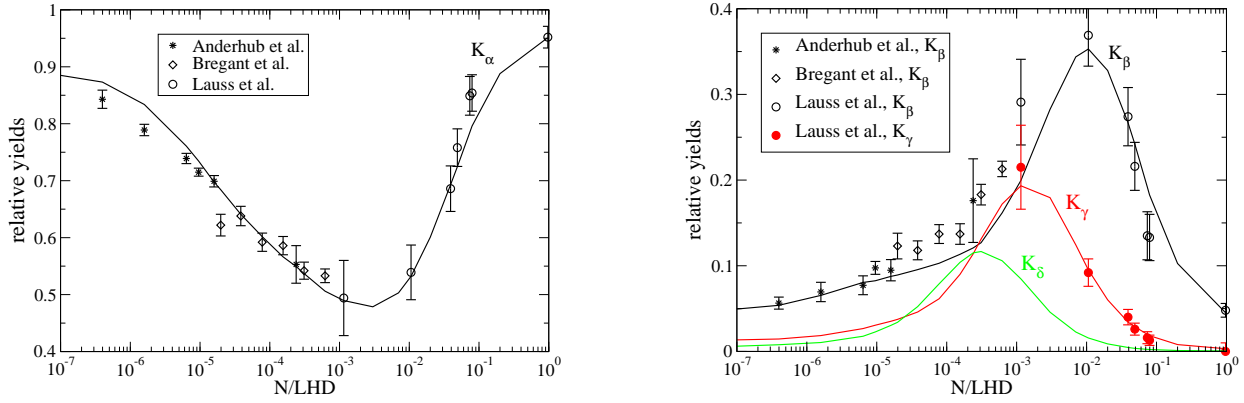


Figure 2: The density dependence of the relative X-ray yields in muonic hydrogen:  $K_\alpha$  on the left;  $K_\beta$ ,  $K_\gamma$  and  $K_\delta$  yields (black, red and green, respectively) on the right. The experimental data are from [16, 17, 18].

The agreement between theoretical results and experimental data is very good practically for all densities under consideration. The observable disagreements can be a subject for further both theoretical and experimental studies. In our opinion, there are also a number of problems which demand more elaborate experimental studies: a proper separation of the different  $k$  lines, inclusion a Doppler broadening effect in the analysis of the experimental data and so on. It would be very important to check the present results directly by measuring the absolute X-ray yields at some values of the target density.

The kinetic energy distribution of the exotic atom changes during the cascade and is a more refined probe of the theoretical approaches to the description of the cascade processes. Using the cascade model described above we calculated the  $\mu^-p$  kinetic energy distribution at the moment of the  $K_\alpha$ ,  $K_\beta$ , etc. radiative transitions and the corresponding Doppler broadening of the  $1s$  line due to the kinetic energy distribution of the exotic atom at the instant of the  $np \rightarrow 1s$  radiative transitions ( $n = 2 \div 4$ ) at the target pressure 10 bar ( $\sim 10^{-2}$  LHD). The results are shown in Figure 3.

As it is seen from Figure 3, the kinetic energy distribution has distinctive high energy structures arising from different Coulomb transitions with  $\Delta n \geq 1$  preceding the radiative de-excitation. The complicated shapes of these structures can be simply explained by the interplay of three factors: the kinetic energy distribution of exotic atom before Coulomb transition, the anisotropy of the angular distribution in the Coulomb de-excitation process and, finally, the deceleration due to the elastic scattering and Stark transitions after Coulomb de-excitation but before the radiative de-excitation.

The energy distribution at low  $n$  can be determined by measuring the Doppler broadening

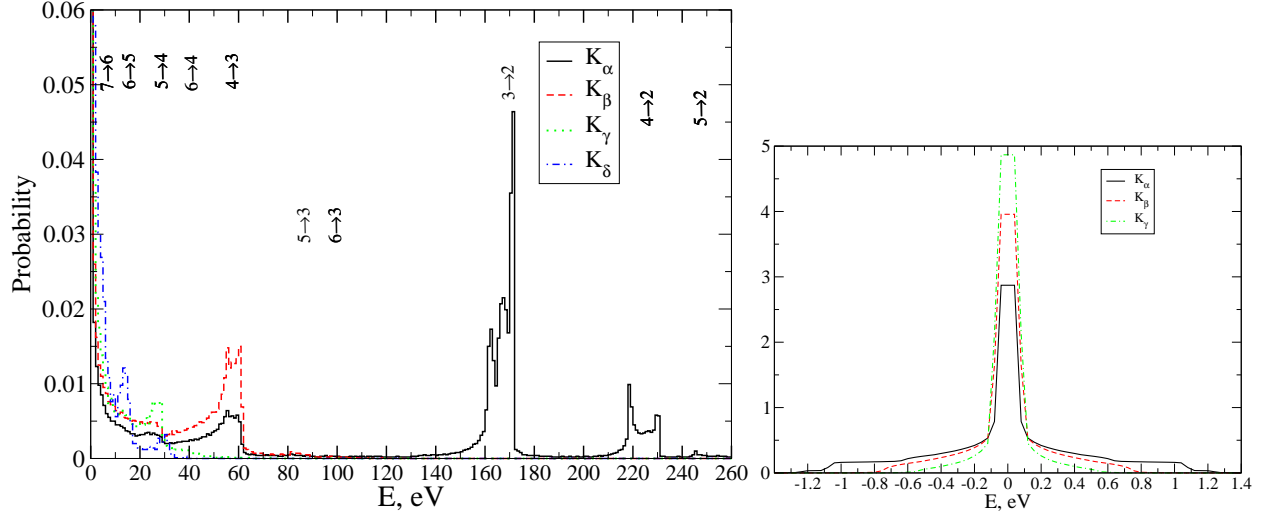


Figure 3: On the left: the kinetic-energy distribution of  $\mu^-p$  at the instant of the radiative  $np \rightarrow 1s$  transitions in gaseous hydrogen at pressure 10 bar. On the right: the  $K$ -line shapes after Doppler broadening due to the kinetic-energy distribution.

of  $K$  X-ray lines. As demonstrated in Figure 3, the high-energy components lead to the significant Doppler broadening, which especially pronounced for  $K_\alpha$  line. The resulting shapes and widths for  $K_\alpha$ ,  $K_\beta$  and  $K_\gamma$  lines at target pressure 10 bar are shown in Fig. 3 (on the right panel). A significant spreading up to  $\pm 1.25$  eV for  $K_\alpha$  line was found.

The essential acceleration during cascade is illustrated in Figure 4. Here the calculated density dependence of the mean kinetic energy at the instant of the radiative  $np \rightarrow 1s$  de-excitation is shown. At the densities from  $10^{-7}$  LHD to  $\sim 2 \cdot 10^{-4}$  LHD the mean energy

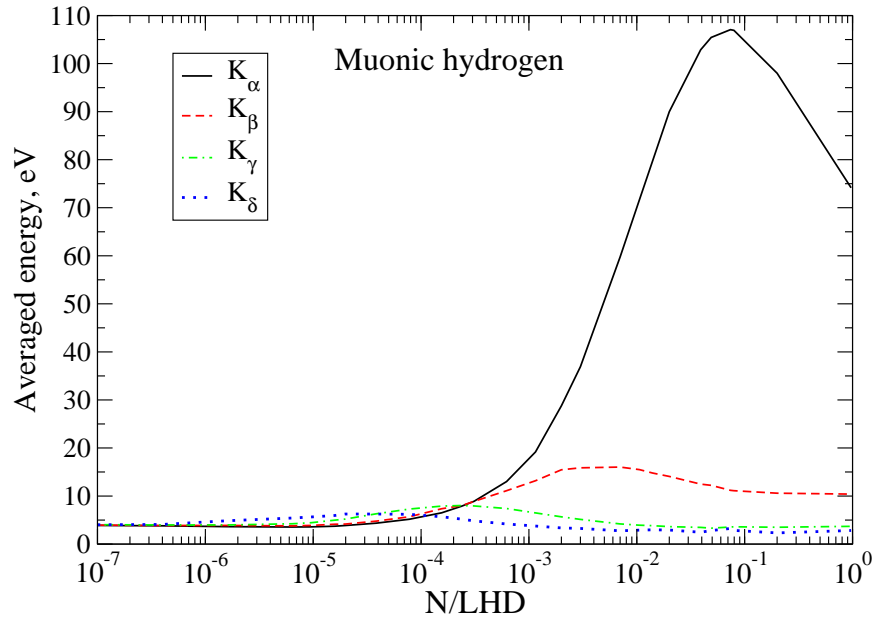


Figure 4: The density dependence of the mean kinetic energy of the  $\mu^-p$  at the instant of the different radiative  $np \rightarrow 1s$  transitions.

slowly increases for all lines and changes correspondingly from 4 eV to 8 eV. At more higher densities the mean energy of the  $K_\beta$  line reaches the maximum value  $\sim 20$  eV in the density interval  $10^{-3} - 10^{-2}$  LHD. The most pronounced increase of the mean energy was obtained for  $K_\alpha$  line with the maximum more than 100 eV at the density  $\sim 8 \cdot 10^{-2}$  LHD.

### 3.2 Pionic hydrogen

The present study of the atomic cascade in pionic hydrogen was focused on the experimental data for the absolute  $X$  ray yields [19] and the neutron time-of-flight spectrum [7] obtained at LHD. The results of our cascade calculations for the absolute  $X$ -ray yields as a function of the target density are shown in Figure 5 in comparison with the experimental data [19]. The nuclear absorption in the hadronic atoms results to a strong suppression of the  $KX$ -ray yields, beginning from very low densities. As a whole the calculated yields are in a good agreement with the experimental data. In the calculation we introduced the additional parameter simulating the induced absorption from  $np$  states. The value of this parameter used in all present calculations for  $2p$ -state was chosen equal to 0.045 meV.

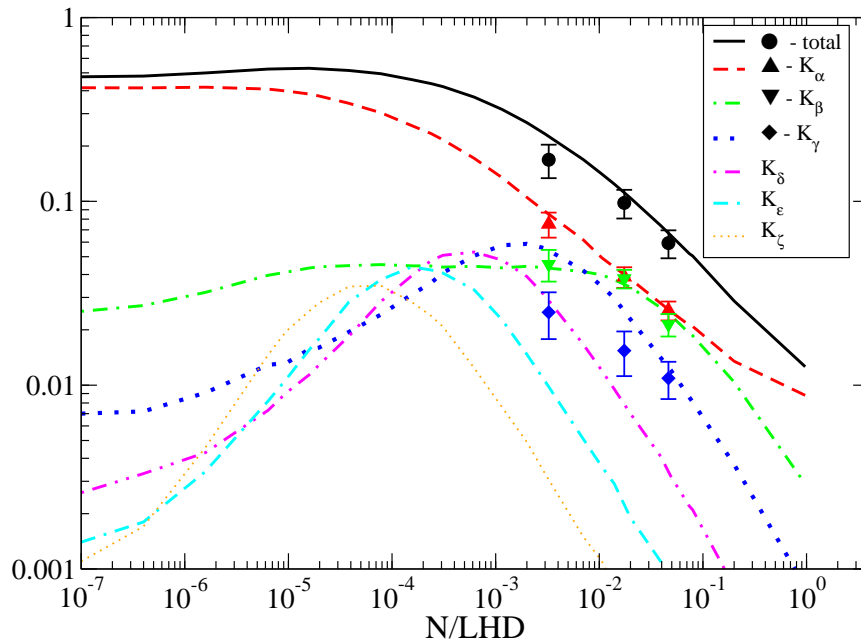


Figure 5: The density dependence of the absolute  $X$ -ray yields in  $\pi^-p$  atom. The experimental data are from [19].

The kinetic energy distribution of the pionic hydrogen at the moment of nuclear absorption in liquid hydrogen is shown in Figure 6. The experimental data from PSI experiments [7] (Bad. and the present theoretical description are shown on the left side and right side of the Figure 7 respectively. The most promising features are that for the first time we can explain in more details both the whole kinetic energy distribution of the  $\pi^-p$  atoms at the instant of charge-exchange reaction and fine structure of this distribution. In particular, according to our calculations the component around  $\sim 105$  eV and  $\sim 209$  eV are explained by the  $5 \rightarrow 3$  and  $3 \rightarrow 2$  Coulomb transitions, respectively. Besides, the relative yields of high energy components at the energies  $\sim 105$  eV and  $\sim 209$  eV are in

good agreement with the experimental data [7]. Thus in contrast to previous theoretical studies the prediction of the present cascade model are in good agreement with the neutron time-of-flight spectrum at LHD.

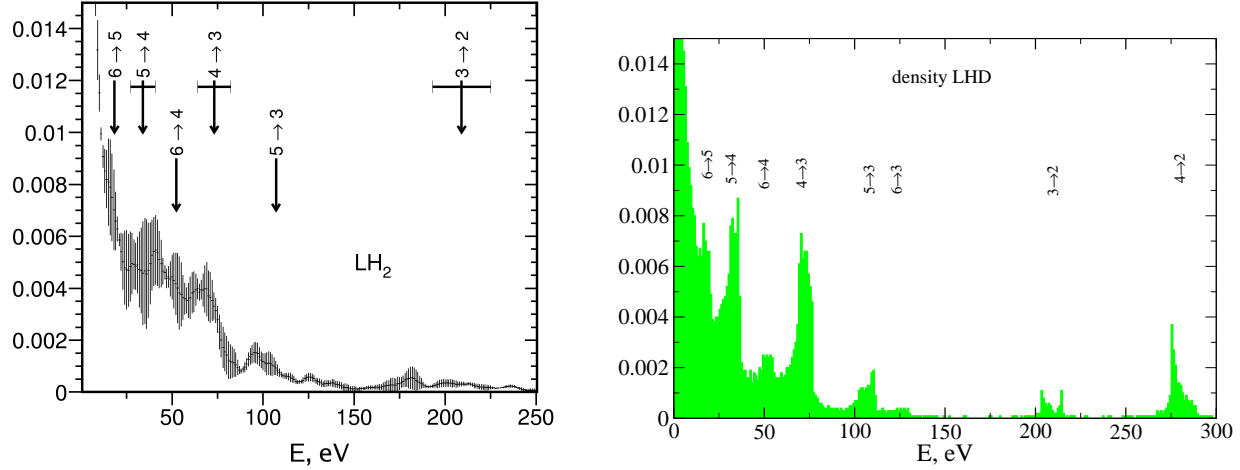


Figure 6: The kinetic energy distribution of  $\pi^-p$  at the instant of the nuclear absorption in liquid hydrogen: the experimental data [7] ( on the left) in comparison with the results of the present cascade calculations (on the right)

In order to illustrate both the importance of the CD transitions with  $\Delta n > 1$  and strength of the CD transitions with  $\Delta n = 1$  the three variants of the cascade calculations were performed: full calculation where all CD transitions are taken into account, the calculation with only  $\Delta n = 1$  CD transitions and, finally, the calculation with  $\Delta n = 1$  CD transitions decreased by factor  $k_{CD} = 0.1$ . The results introduced in Figure 7 show that in contrast to the CC approach [12, 13] the previous theoretical description of the CD process in the semiclassical [20] and advanced adiabatic approaches (see [21] and references therein) are in disagreement with the experimental data [7].

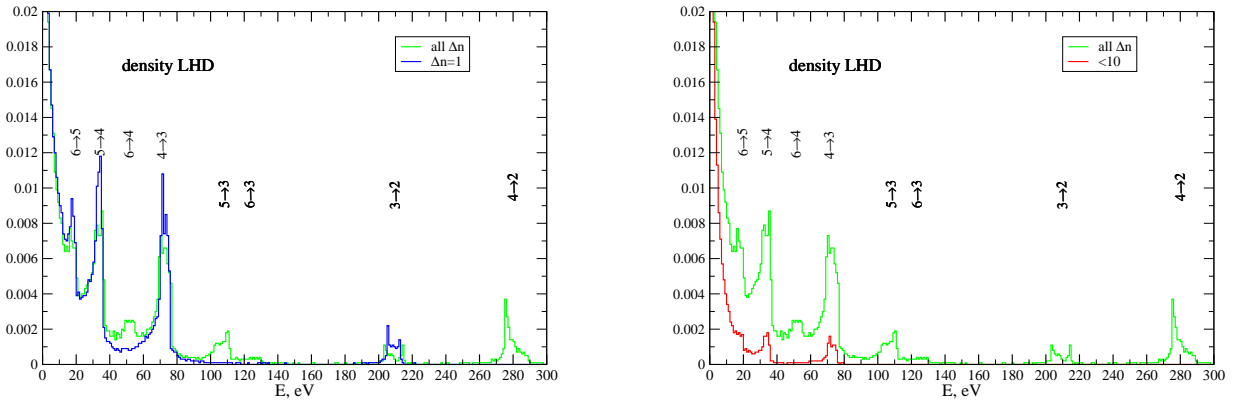


Figure 7: The kinetic energy distribution of  $\pi^-p$  at the instant of the nuclear absorption in liquid hydrogen for the different variants of the Coulomb transitions: full calculation - green line and only  $\Delta n = 1$  CD transitions - blue line (on the left side); full calculation - green line and only  $\Delta n = 1$  with the factor  $k_{Cd} = 0.1$  - blue line (on the right side)

## 4 Conclusion

The present version of the cascade model significantly improves the previous cascade calculations due to the self-consistent treatment of the elastic scattering, Stark transitions and Coulomb de-excitation. The inclusion in the cascade code the results of the detailed quantum mechanical calculations of the differential and integral cross sections for  $nl \mapsto n'l'$  collisional transitions allowed us to describe the kinetics of the atomic cascade without employing any fitting parameters and more accurately.

The predictions of this cascade model are in a good agreement with the experimental data both for muonic and pionic hydrogen atoms. In particular, the present cascade calculations allow for the first time to explain the observed kinetic energy distribution of  $\pi^-p$  atoms at the instant of nuclear reaction. Our results explain the high energy components around  $\sim 105$  eV and  $\sim 209$  eV (due to  $5 \rightarrow 3$  and  $3 \rightarrow 2$  Coulomb transitions) and lead to a very good agreement with the experimental weights of these components.

## 5 Acknowledgements

The authors would like to thank L. Simons who initiated this investigation as well as D. Gotta, F. Kottmann, V. Markushin and D. Taqqu for many fruitful and stimulating discussions. This work was supported by Russian Foundation for Basic Research Grant No. 06 – 02 – 17156.

## References

- [1] D. Gotta, Prog.Part.Nucl.Phys. **52**, 133 (2004).
- [2] M. Leon, H.A. Bethe, Phys.Rev. **127**, 636 (1962).
- [3] E. Borie, M. Leon, Phys.Rev. A **21**, 1460 (1980).
- [4] T.P. Terada, R.S. Hayano, Phys.Rev. C **55**, 73 (1997)73.
- [5] J.F. Crawford *et al.*, Phys.Rev. D **43**, 46 (1991).
- [6] D.J. Abbot *et al.*, Phys.Rev. A **55**, 165 (1997).
- [7] A. Badertscher *et al.*, Europhys. Lett. **54**, 313 (2001).
- [8] F. Kottman *et al.*, Hyperf.Interact. **119**, 3 (1999); 138(2001)55.
- [9] R. Pohl *et al.*, Hyperf. Interact. **138**, 35 (2001).
- [10] V.E. Markushin, Phys.Rev. A **50**, 1137 (1994).
- [11] T.S. Jensen, V.E. Markushin, Eur.Phys. J. D **21**, 271 (2002).
- [12] G.Ya. Korenman, V.N. Pomerantsev, and V.P. Popov, JETP. Lett. **81**, 543 (2005).
- [13] V.N. Pomerantsev, V.P. Popov, JETP. Lett. **83**, 331 (2006); Phys. Rev. A **73**, 040501-1 (2006).
- [14] G.Ya. Korenman, Hyperf. Interact. **101/102**, 81 (1996).
- [15] J.S. Cohen, Rep. Prog. Phys. **67**, 1769 (2004).
- [16] H. Anderhub *et al.*, Phys. Lett. B **143**, 65 (1984).
- [17] N. Bregant *et al.*, Phys. Lett. A **241**, 344 (1998).
- [18] B. Lauss *et al.*, Phys. Rev. Lett. **80**, 3041 (1998).



- [19] A.J. Rusi El Hassani *et al.*, Z. Phys. A **135**, 113 (1995).
- [20] L. Bracci, G. Fiorentini, Nuovo Cimento A **43**, 9 (1978).
- [21] A.V. Kravtsov, A.I. Mikhailov, Yad. Fiz. **69**, 395 (2006).